Investigating the fouling layer of polyamide nanofiltration membranes treating two different natural waters: internal heterogeneity yet converging surface properties

G. Makdissy, P. M. Huck, M. M. Reid, G. G. Leppard, J. Haberkamp, M. Jekel and S. Peldszus

ABSTRACT

This study investigated the fouling of four polyamide nanofiltration membranes by two surface waters that differed substantially in major properties. The emphasis was on determining the characteristics of the fouling layer on the membranes. The rates of fouling for the two waters differed considerably, with a more rapid flux decline being observed for the water having higher biopolymer and major ion concentrations. Measurements of membrane roughness, contact angle and zeta potential in general showed considerable differences for each of these properties among the virgin membranes. However, values of each of these parameters tended to converge for all membranes after fouling, regardless of which water had been used. This result is very significant (for example for the removal of trace contaminants, which in many cases may depend on membrane properties) because in practice a membrane spends virtually all of its operating life fouled to some degree. Several techniques including transmission electron microscopy (TEM) were used to conduct detailed investigations of the fouling layer. These results demonstrated the great heterogeneity within that layer, despite the similar overall properties mentioned above. This heterogeneity is significant for quantitative understanding of the relationship between fouling and flux and for strategies to reduce or remove fouling.

Key words | atomic force microscopy, biopolymers, contact angle, fouling, nanofiltration, transmission electron microscopy

G. Makdissy
P. M. Huck (corresponding author)
S. Peldszus
NSERC Chair in Water Treatment,
Department of Civil and Environmental Engineering,
University of Waterloo,
200 University Avenue West,
Waterloo, Ontario N2L 3G1,
Canada
Tel.: +1-519-888-4567 x32707
Fax: +1-519-746-7499
E-mail: *pm2huck@uwaterloo.ca*

M. M. Reid
Faculty of Health Sciences Electron Microscopy Facility, McMaster University,
1200 Main Street West,
Hamilton, Ontario L8N 3Z5,
Canada

G. G. Leppard
National Water Research Institute,
Environment Canada,
Burlington, Ontario L7R 4A6,
Canada

J. Haberkamp
M. Jekel
Department of Water Quality Control,
Technical University of Berlin,
Sekr. KF 4, Strasse des 17. Juni 135,
10623 Berlin,
Germany

INTRODUCTION

Nanofiltration (NF) is gaining wider use in various applications, including drinking water production. As with all membranes, fouling remains a major issue for NF use. NF membranes in full-scale operation are exposed to various types of fouling, namely inorganic, organic, colloidal and bio-fouling. In practice, a membrane spends virtually all of its operating life fouled to at least some extent. Therefore, a better understanding of the properties of fouled membranes is important.

doi: 10.2166/aqua.2010.062

The factors that control fouling include membrane properties, water composition and hydrodynamic conditions. With respect to membrane properties, surface roughness has been found in some investigations to play a key role. Hobbs *et al.* (2006) showed that NF membrane fouling became more severe with increasing surface roughness. Similarly, Li *et al.* (2007) found that membrane surface roughness had an important effect on RO membrane fouling by biopolymers. In contrast, Tang *et al.* (2007) found that

membrane flux performance was largely independent of virgin NF membrane properties but depended on hydrodynamic conditions, flux and crossflow velocity (CFV). While lowering CFV affected flux performance moderately, severe flux reduction occurred at high initial flux. Hong & Elimelech (1997) have highlighted the importance of water-quality parameters, particularly the role of divalent calcium ion in increasing flux decline. Texeira & Rosa (2006) also pointed out a decrease in flux in the presence of calcium.

Many researchers have undertaken work to identify the nature of foulants. Huang *et al.* (2007), in investigating four low-pressure hollow fibre membranes and four different waters, found that the water (i.e. the source of natural organic matter (NOM)) played a primary role in fouling. Amy & Cho (1999) identified polysaccharides as dominant foulants in UF (ultrafiltration) and NF filtration of surface waters. Mackey (1999) studied the fouling of UF and NF membranes by various model compounds such as polysaccharides, polyhydroxyaromatics and proteins. Those authors found that larger compounds (polysaccharides and proteins) caused more fouling, and in mixtures the fouling increased. Similarly, Li *et al.* (2007) observed a considerable synergistic fouling effect when model biopolymers, bovine serum albumin (BSA) and sodium alginate co-existed in the feed of a reverse osmosis (RO) membrane. Her *et al.* (2007) found that protein- and polysaccharide-like substances were major foulants of an NF membrane fed with sand-filtered and ozonated sand-filtered water. Thus, it is evident that biopolymer fractions of organic matter are important for NF/RO fouling.

In terms of the properties of fouled membranes, Xu *et al.* (2006) found an increase of surface roughness upon fouling of smooth membranes, while a decrease was observed with rough membranes. Cho *et al.* (2000) reported that NOM fouling caused a decrease in hydrophobicity of hydrophobic membranes and an increase for hydrophilic membranes. Roudman & DiGiano (2000) reported a significant increase in hydrophobicity for NF membranes after adsorption of NOM. Yuan & Zydney (2000) attributed an observed reduction in zeta potential after adsorption of humic acid to its lower charge density, compared to the membrane surface. Cho *et al.* (2000) reported that NOM fouling also caused a reduction in the membrane's negative surface charge.

Yamamura *et al.* (2007) observed changes over time in the organic and inorganic composition of the fouling layer of a microfiltration membrane and used atomic force microscopy (AFM) to investigate changes in membrane morphology. Tran *et al.* (2007) investigated the fouling layer of a spiral wound reverse osmosis (RO) membrane treating a brackish water. They determined both organic and inorganic constituents and found differences in both of these as a function of depth in the fouling layer. From this they deduced that fouling had developed through different stages. Her *et al.* (2007) used various techniques to analyse their fouled NF membrane, but did not include transmission electron microscopy (TEM).

A number of the studies cited above have used model compounds; however, because fouling is a very complex process, it cannot be captured in its entirety by such investigations. Some investigations have targeted actual source waters; however, in a number of these cases only a single water and/or membrane type were used. The present study investigated fouling by two different surface waters, each fed to four different NF membranes. Although rates of fouling were measured and differences interpreted to the extent possible, the real objective of the investigation was to characterize the properties of the fouled membranes using a variety of techniques, and to interpret the significance of the results for practice.

METHODS AND MATERIALS

Membranes and characterization

Initially, ten commercially available NF membranes were screened, from which four were chosen for further study: NF90, NF270 (both from Dow Filmtec, Minneapolis, MN), HL (GE Osmonics, Minnetonka, MN) and SR2 (Koch Membrane Systems, San Diego, CA). All four were thin-film composite membranes having a three-layered structure comprised of a non-woven fabric, a porous polysulfone support and an active polyamide layer. Prior to characterization, the virgin membrane specimens were first soaked in ultrapure water for a minimum of 24 hours (the ultrapure water was replaced three times), then pre-compacted overnight and air-dried.

Membrane surface morphology was characterized by AFM in tapping mode using MultiMode AFM (Veeco, SFR, Kanata, ON, Canada). The cantilever was made of etched silicon (Si) with a spring constant of 20–80 N/m and a nominal tip apex radius of 5–10 nm. After scanning, the images were plane-fitted and flattened with a second-order polynomial approximation to remove scanner-induced curvature and slope. Membrane surface roughness was quantified using average roughness, which is defined as the arithmetic average of the absolute values of the surface height deviations measured from the centre plane. Three different scans were used: 0.5 μm × 0.5 μm, 1 μm × 1 μm and 5 μm × 5 μm with a resolution of 512 × 512 points. Three images were taken for each scan at different spots and an average of roughness values was reported.

The thickness and nanoscale morphology of the active layer were determined using TEM. Portions of each membrane were prepared for ultrathin sectioning using a protocol that involved a primary fixation in buffered glutaraldehyde plus ruthenium red, followed by subsequent processing (including an osmication step) and then embedding in a low-viscosity epoxy resin. (Details and the rationale for the overall approach are provided in Liss *et al.* 1996). The ultrathin sections (80 nm thick) were cut with a diamond knife mounted in a Leica Ultracut UCT ultramicrotome (Leica Mikrosysteme, Vienna, Austria). A comprehensive treatment of the use of TEM preparatory protocols and instrumentation, and the rationale for selecting a specific protocol for a specific research need is found in Mavrocordatos *et al.* (2007), accompanied by guidelines on how to detect, assess and minimize artefacts. Ultrathin sections, placed on Formvar-covered copper grids, were observed and documented by a JEOL JEM 1200 EX TEMSCAN scanning/transmission electron microscope, or STEM (JEOL, Peabody, MA, USA) operated at an accelerating voltage of 80 kV. On a 'per particle' basis, energy-dispersive spectroscopy (EDS) was used to identify elements (Chandler 1977) and to assess the relative abundances (Jackson & Leppard 2002) of pertinent elements ($Z > 10$) detected in both virgin and fouled membranes. EDS spectra were obtained using a Tracor Northern X-ray detector (Noran, Madison, WI, USA) and EDS 2004 microanalysis software (IXRF Systems Inc., Houston, TX, USA). To guarantee representativity, all morphological and spectromicroscopical analyses were based on the systematic search protocol of Leppard *et al.* (2003) for representative images.

Membrane surface charge was measured as zeta potential using two Electro Kinetic Analyzers; namely Bi-EKA (Brookhaven Instruments, Holtsville, NY, USA) and SurPASS (Anton-Paar, Graz, Austria). Measurements were performed using the streaming potential method according to the Fairbrother-Mastin approach, with a clamping cell at room temperature (25°C) in 0.01 M NaCl at pH 7. For each measurement a membrane surface was clamped against a polymethyl methacrylate (PMMA) spacer.

Membrane hydrophobicity was analysed by contact angle measurement, performed with two instruments: an ASTVCA2500 XE (Systems for Research, Canada) and a DSA 100S (Kruss, Hamburg, Germany) in a three-phase system consisting of the membrane surface, air and an ultrapure water droplet of 6 μL. Contact angle was measured using the sessile drop method on three membrane samples and an average value was calculated.

Although the active layers of the four selected membranes were similar in chemical composition, they differed in a number of other characteristics (Table 1). The molecular weight cut-off (MWCO) and pore size of the NF90 membrane were the smallest. The SR2 membrane had the largest MWCO and pore size, whereas values for HL and NF270 membranes (where information is available) lay in between. The surface roughness and thickness of the NF90 active layer were much greater than the corresponding values for the other membranes. A strong correlation ($r^2 = 0.98$) was found between active layer roughness and thickness, indicating that in this respect AFM and TEM are complementary. All membranes had a negative surface charge (as determined by zeta potential) as a result of dissociation of the functional groups on the membrane surface or the adsorption of ions from solution. The NF270 membrane had by far the highest zeta potential. The contact angles for the SR2, NF270 and HL membranes all lay within a narrow range 49–58°, while the much higher contact angle for NF90 (73°) indicates much greater hydrophobicity for that membrane.

Feed waters

In order to assess the impact of feed water characteristics on fouling, two Canadian surface waters, the Grand River

Table 1 | Characteristics of the selected virgin NF membranes

Parameter	NF90	HL	NF270	SR2
Active layer structure*	Fully aromatic	Aromatic/aliphatic	Aromatic/aliphatic	N/A
Active layer make-up*	1,3 phenylene diamine + tri acid chloride of benzene	N/A	Piperazine + tri acid chloride of benzene	N/A
MWCO (Da)*	200	150–300	400	400–700
Average pore diameter (nm)†	0.68	N/A	0.84	1.28
PSD (nm)‡	Unimodal (0.81)	Bimodal (1.02, 1.77)	Bimodal (0.90, 1.56)	N/A
Average roughness (nm)§	29 ± 6	2 ± 0	4 ± 1	12 ± 1
Active layer thickness (nm)‖	138 ± 33	13 ± 3	14 ± 1	48 ± 13
Zeta potential (mV)¶	−15.19 (−5.72)	−7.33 (−4.62)	−41.03 (−29.46)	−16.57 (−6.06)
Static contact angle (degrees)**	73 ± 2 (73 ± 1)	52 ± 2 (52 ± 2)	49 ± 2 (48 ± 2)	49 ± 2 (58 ± 6)

N/A, not available.
*Manufacturer's data.
†Nghiem *et al.* (2004).
‡PSD: Pore Size Distribution, Košutić *et al.* (2006).
§Tapping mode, scan size 5 μm × 5 μm, the values are the average of 30 measurements (10 measurements/image).
‖Thickness values are the average of 60 measurements (20 measurements/image).
¶Streaming potential method, pH 7, 25°C, 0.01 M NaCl. Values were obtained using the Bi-EKA instrument. The uncertainty is ±0.5 mV. Values in parentheses were obtained using the SurPASS instrument; the difference between the two sets of data is due to the different geometry of the streaming channel of the two instruments.
**Sessile drop method, measurement performed using VCA2500 XE instrument once the drop (volume 6 μL) had touched the surface of the membrane. The values represent an average of 6 measurements (2 measurements/image). Values in parentheses were obtained with the DSA 100S instrument after 30 s. They represent an average of 4 measurements (2 measurements/image).

(Kitchener-Waterloo, Ontario) and the French River (Tatamagouche, Nova Scotia) were used. These two waters are designated GRW and FRW respectively. The Grand River is heavily impacted by urban and agricultural activities including waste water treatment effluents, whereas the French River is impacted by urban and agricultural activities. Since in practice source waters are pre-treated prior to NF, both waters were pre-filtered through a mixed cellulose ester membrane (0.45 μm, GN-6 Metricel, Pall, East Hills, NY, USA) followed by a polyethersulfone membrane (0.2 μm, Pall) to remove particles larger than 0.2 μm. The pre-filtered surface waters were then spiked with a mixture of seven organic micropollutants, each at a concentration of 1 μg/L, and fed to the NF bench-scale crossflow filtration unit. The spiking was done to investigate the impact of fouling on the removal of contaminants (Makdissy *et al.* in preparation). These results are not discussed in this paper and the spiking is mentioned here only for completeness. The spiked concentrations, approximately three orders of magnitude lower than the background total organic carbon (TOC) concentration, were not considered to have had an impact on the fouling behaviour.

Prior to fouling tests, feed water samples were characterized in terms of pH, dissolved organic carbon (DOC), ultraviolet absorbance at 254 nm (UV_{254}), conductivity, cations, anions and organic carbon distribution. pH was measured using an Orion pH meter (Orion Research Inc., MA, USA). DOC was measured using an O.I. 1010 Analytical TOC analyser (Standard Method #5310). UV_{254} was measured using a Hewlett-Packard 8453 spectrophotometer (Standard Method #5910) with a 1-cm quartz cell. Conductivity was measured using a CO 150 Hach electrical conductivity meter (Standard Method #2510). The concentrations of silica and major cations were measured by a commercial laboratory (Standard Method #200.8). The concentration of anions was measured using a Dionex ion chromatograph utilizing an IonPac AS-SC column.

The characteristics of the pre-filtered feed waters are summarized in Table 2. Substantially higher concentrations of most major ions were observed in GRW than in FRW, which is consistent with their respective conductivities. GRW has also a higher DOC concentration; however, its specific UV absorbance SUVA is slightly lower.

Table 2 | Feed water characteristics

Water	Sampling date	pH	DOC (mgC/L)	SUVA (L/mgC m)	Cond. (μS/cm)	SiO_2 (mg/L)	Na_{total} (mg/L)	Ca_{total} (mg/L)	Fe_{total} (mg/L)	Mg_{total} (mg/L)	Mn_{total} (mg/L)	Cl^- (mg/L)	NO_3^- (mg/L)	SO_4^{2-} (mg/L)
GRW	April-16-2007	7.69	5.66*	2.81*	500*	5.2*	16.9*	61.4*	<0.05	15.6*	0.012*	32.6*	17.1*	18.1*
			5.68†	2.82†	500†	4.6†	17.6†	51.6†	<0.05	16.0†	0.008†	29.0†	14.9†	16.6†
FRW	June-19-2007	6.93	3.60*	2.92*	80*	4.6*	4.7*	8.8*	<0.05	1.1*	0.001*	7.4*	1.6*	4.7*
			3.05†	3.51†	90†	4.8†	6.6†	9.9†	<0.05	1.4†	0.002†	6.5†	0.3†	2.9†

Cond., conductivity.
*Data for the NF90 and NF270 feed water.
†Data for the HL and SR2 feed water.

High-performance liquid (size exclusion) chromatography (LC) with on-line UV absorbance at 254 nm and a DOC detector (LC-OCD system by DOC-Labor Dr. Huber, Karlsruhe/Germany; SEC column: Toyopearls HW-50S by Tosoh Bioscience, Tokyo/Japan) was employed to characterize the organic matter in the two waters following the approach of Haberkamp *et al.* (2007). A detailed description of the biopolymer identification and quantification can be found in the Supporting Information of Hallé *et al.* (2009).

The water samples were maintained at room temperature (25°C) during the analyses. All of the above measurements were also performed on the membrane permeates; however, only the results for the inorganic ions are discussed herein.

Fouling tests

As was done for membrane characterization, membrane coupons (14.6 cm × 9.5 cm) were first soaked in ultrapure water (the ultrapure water was replaced three times) for a minimum of 24 hours before being loaded into the bench-scale crossflow filtration unit (Sepa II, GE-Osmonics, Minnetonka, MN, USA). Two units were utilized: NF90 was run simultaneously with NF270 and HL simultaneously with SR2. A feed spacer ~1.2 mm thick was placed in each unit. While both units shared the same feed tank, they were hydraulically independent through the use of one hydra cell pump per unit (Wanner Engineering, Minneapolis, MN). Stainless steel and Teflon® were used throughout to minimize adsorption of foulants/contaminants to the unit. Prior to fouling tests, the membranes were compacted overnight using ultrapure water.

Studies by Li *et al.* (2007) and Tang *et al.* (2007) have highlighted that initial flux, rather than applied pressure, seem to directly affect the extent of flux reduction in NF and RO membranes. Thus, in the present investigation different operating pressures, namely 150, 134, 105 and 100 psi were used for NF90, HL, NF270 and SR2 membranes respectively, to obtain the same initial permeate flux of 108 L/h m^2. Crossflow velocity has also been found to be an important factor controlling fouling. In practice, typical velocities in spiral-wound elements range from 0.05 to 1.5 m/s (Allgeier & Summers 1995). For the present investigation, an initial crossflow velocity of 0.09 m/s, corresponding to a feed flow of 500 mL/min and a Reynolds Number (Re) of 100 (spacer-filled channel), was chosen. The resulting initial recovery defined as the ration of permeate flow to feed flow was 5%.

The experiments were performed in recycle mode, in which retentate and permeate were returned to the feed water tank. The feed water temperature was kept at 20° ± 5°C throughout each experiment using a chiller (Polyscience, Niles, IL, USA) with digital temperature control. Filtration tests were carried out for 4 days and 3.5 days with GRW and FRW, respectively.

Fouled membrane autopsy and information on foulants

Membrane autopsy consisted of subjecting the dry fouled membrane specimens to AFM, TEM, hydrophobicity and surface charge analyses. With respect to TEM, all fouled membranes were stabilized and prepared for analysis according to a fixation protocol (Liss *et al.* 1996) designed to detect and help characterize deposited foulants (Liao *et al.* 2004). EDS analysis of the dry fouled membrane specimens also provided information on the fouling materials. Supporting information was provided by measuring conductivity and major ion concentrations in the permeate samples.

RESULTS AND DISCUSSION

Flux decline and DOC loading

Figure 1 shows permeate flux as a function of cumulative DOC loading (DOC delivered per unit membrane area; calculated by multiplying specific volume with the DOC of the feed) to account for the difference in DOC concentrations of the two feed waters (Table 2). For FRW a sharp decrease in flux was observed with NF90 and HL membranes. Although this was possibly caused by pore restriction and initial deposition of the foulants on the membrane surface, as reported by Van der Bruggen & Vandecasteele (2001), confirmation of the exact mechanism was outside the scope of the present investigation. For the NF270 and SR2 membranes, a gradual decrease in flux was observed over the entire run. This is an indication that no or limited pore restriction takes place, possibly due to the membranes' larger MWCO/pore size (Table 1).

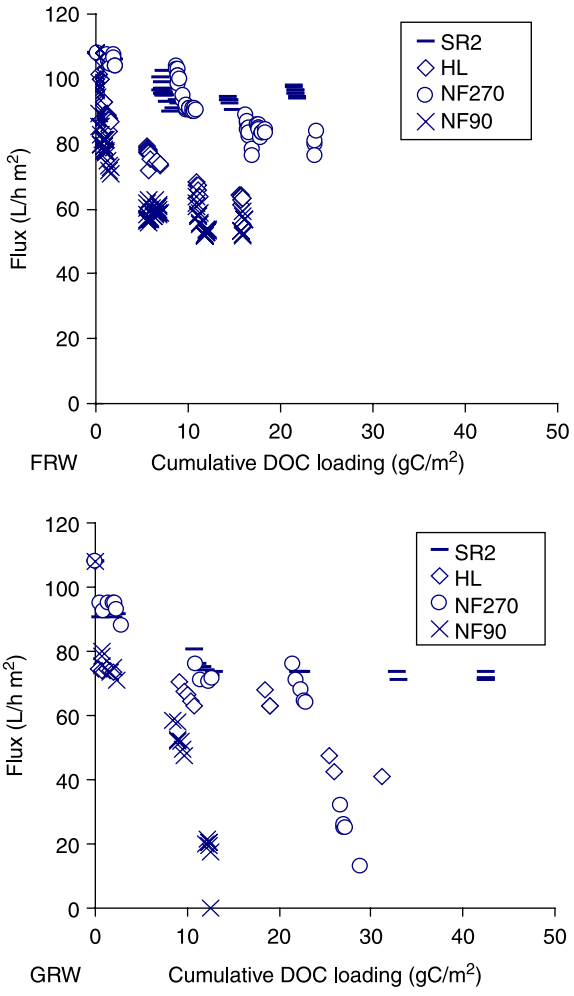

Figure 1 | Permeate flux versus cumulative DOC loading.

For GRW, a continuous decrease of flux was observed with all membranes (except SR2, which exhibited a similar fouling trend to the one for this membrane fed with FRW). The observed flux declines at the end of the 4 days' fouling tests with GRW were inversely correlated ($r^2 = 0.84$) with DOC loading. This is as expected, because a greater flux decline during the test led to less DOC delivery to the membrane.

The overall flux decline rates follow the order of NF90 > NF270 ≥ HL > SR2 and NF90 > HL > NF270 > SR2 for GRW and FRW respectively, indicating that, in general, the membrane with a smaller MWCO is more prone to fouling than the membrane with a larger MWCO. Although this result is as would be expected, different results were reported by Nghiem & Hawkes (2007), who studied the fouling of NF membranes at the same initial flux using humic acid as a model organic foulant. Those authors reported more fouling with the larger pore sizes membranes due to the greater effect of adsorption and pore restriction. An important difference with our results is that our natural waters contained a range of organic foulant material, as discussed later. Although as mentioned above a correlation was found between fouling rate and membrane pore size, none was found between fouling rate and any of the other virgin membrane properties (results not shown for reasons of space).

Figure 2 compares fouling (expressed as flux decline) for all four membranes in GRW vs. FRW at a DOC loading of 10 g C per m^2 membrane surface area. It is evident that, at the same DOC loading, the extent of fouling was higher for all membranes when fed with GRW. This is possibly caused by the considerably higher calcium concentration in GRW (52–61 mg/L) than in FRW (9–10 mg/L). In this regard, our observations are consistent with those for model organic compounds (Hong & Elimelech 1997; Lee & Elimelech 2006). However, in studying UF filtration of secondary waste water effluent, Haberkamp (2008) found that a natural calcium concentration of 80 mg/L caused less organic fouling than secondary effluent without calcium. This effect was attributed to the formation of a more

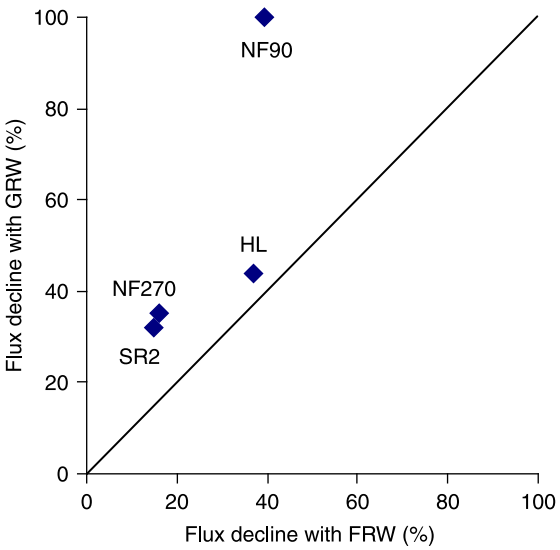

Figure 2 | Comparison of flux decline at 10 gC/m^2 loading for GRW and FRW.

structured fouling layer on the membrane surface with higher permeability to water in the presence of calcium, which acts as a bridging agent between fouling-causing biopolymer molecules. Given the measurable biopolymer concentrations in GRW (presented later), the higher fouling rate for that water cannot necessarily be attributed only to the higher calcium concentration.

A more probable explanation for the difference in the extent of fouling by our two natural waters is the difference in composition of their organic matter. Although many earlier studies suggested that humic substances were the main foulants, more recent investigations have shown that hydrophilic, non-humic, dissolved, colloidal NOM may be a more significant foulant for NF membranes (Ye *et al.* 2005). Although the major foulants for different types of membranes may be different, the importance of biopolymers for fouling with GRW was demonstrated in a previous investigation using UF membranes (Hallé *et al.* 2009).

The organic matter present in both feed waters was characterized using LC-OCD, as described previously. As an example, Figure 3 shows DOC and UV LC-OCD chromatograms for the samples of the two waters that were used for the simultaneous experiments with the NF90 and NF270 membranes. For GRW, the first peak (I) is present only as a small DOC signal with an even smaller UV response. This peak is attributed (e.g. Haberkamp 2008) to biopolymers, i.e. proteins and protein-like material and polysaccharides. The sharp DOC signal (II) with a high corresponding UV response is attributed to humic substances. In FRW, no or very low concentrations of biopolymers were detected (Figure 3B). The detected low UV response around 40 min may reflect the presence of protein-type molecules. (Note that polysaccharides are not detected by UV.) Similar observations were made for the HL and SR2 feed waters (data not shown).

In a recent study Lankes *et al.* (2009) inferred that LC-OCD analyses underestimate the concentration of polysaccharides, which are generally considered to be a major component of peak I. If this occurred in our samples, it is reasonable to conclude that both waters would be impacted to a generally similar degree, assuming that the ratio of

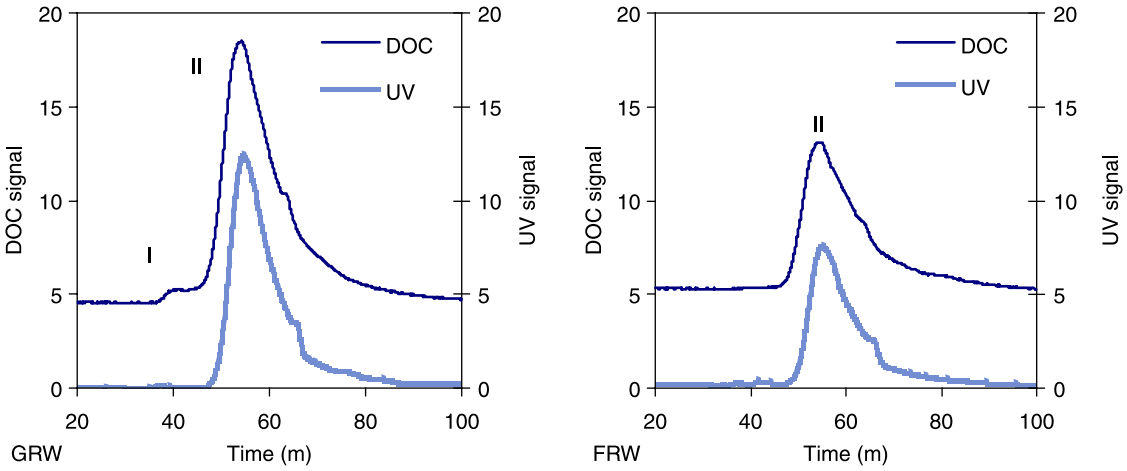

Figure 3 | DOC and UV chromatograms of GRW and FRW.

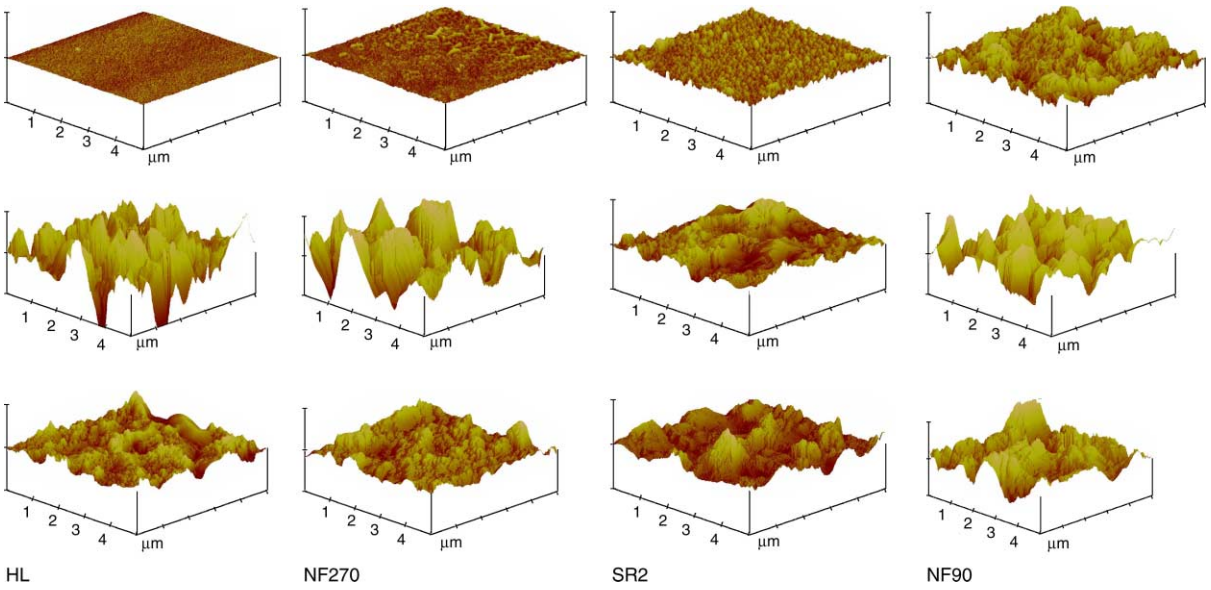

Figure 4 | AFM images (45° view) of virgin (top) and fouled membranes fed with GRW (middle) and FRW (bottom) (scan area 5 μm × 5 μm).

proteins to polysaccharides is generally the same. This would imply that the difference in character observed for the two waters was in fact real.

Membrane properties after fouling

To visualize the fouling effects on membrane morphology, AFM images (Figure 4) for a 5 μm × 5 μm scan size were taken before and at the end of the fouling tests. The difference in surface morphology between virgin membranes is obvious and consistent with the roughness data reported in Table 1. After fouling, the morphology of the membranes changes significantly and is dominated by the build-up of the fouling layer. The presence of the fouling layer was confirmed by visual observation at the end of each experiment, at which time a brown layer of materials was observed firmly attached to the membrane surface with one exception, the loose materials attached to the surface of HL membrane fed with GRW. The increase in average roughness (Figure 5) confirms as well the build-up of the fouling layer. However, a detailed comparison among the various images after fouling in Figure 4 is complicated by the fact that the DOC loading at the end of the fouling tests was different for each membrane (Figure 1).

Analysis of the fouled membranes showed an increase in contact angle (i.e. hydrophobicity) for all (Figure 6), except NF90 fed with GRW, indicating the adhesion of hydrophobic type foulants. Except for this last case, a similar contact angle was observed for all fouled membranes. This similar hydrophobicity indicates a similar fouling layer, and that the surface properties of this layer supplant those of the virgin membrane. Our results showing a convergence of contact angles are consistent with those of Cho *et al.* (2000), who reported that NOM fouling caused a

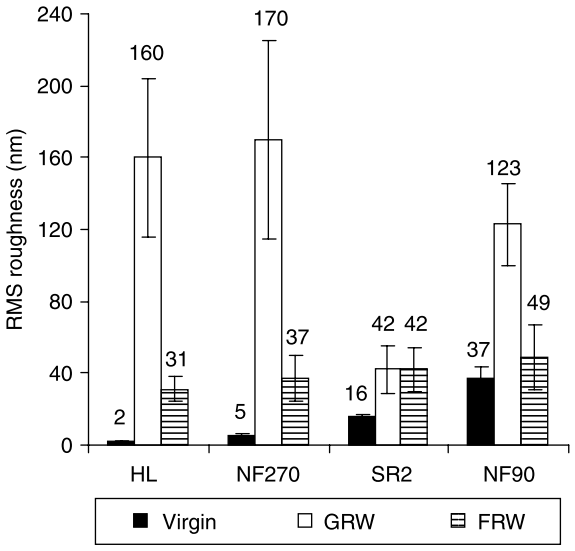

Figure 5 | RMS roughness of virgin and fouled membranes fed with GRW and FRW.

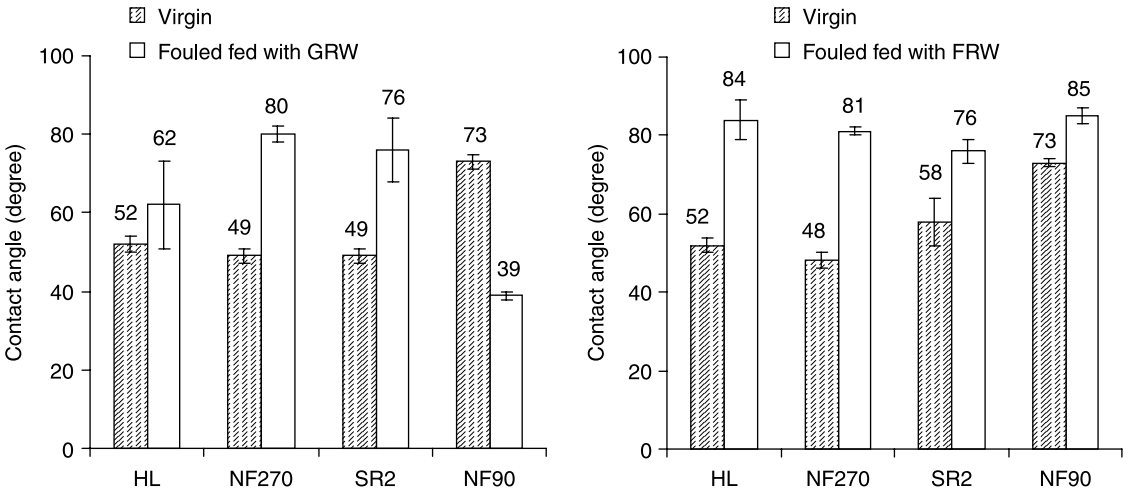

Figure 6 | Contact angle of virgin and fouled membranes fed with GRW and FRW (data on left graph were determined using VCA2500 XE, those on right graph were determined using DSA 100S).

decrease in hydrophobicity of hydrophobic membranes and an increase for hydrophilic membranes.

In terms of zeta potential, the virgin NF270 membrane had a much higher negative value than the other membranes (Figure 7). Filtration with either water shifted the zeta potential of this membrane to less negative values. This is consistent with results reported by Yuan & Zydney (2000) for adsorption of humic acid and by Cho *et al.* (2000) for NOM fouling. However, the zeta potentials of our other three membranes were shifted to more negative values, indicating that a uniform response cannot always be expected. The reason for the increase in charge for FRW is hypothesized to be the deposition of humic substances which contain large moieties of carboxylic acid functional groups, imparting a negative charge to the foulant layer. The shift in zeta potential was negligible for GRW. A possible explanation is that calcium associates or complexes with carboxylic acid functional groups. The deposited foulant layer could therefore have a low negative charge. A more quantitative explanation is complicated by the fact that, for reasons of instrument access and as indicated in Figure 7, two different instruments were used to measure zeta potential for experiments with the two different waters.

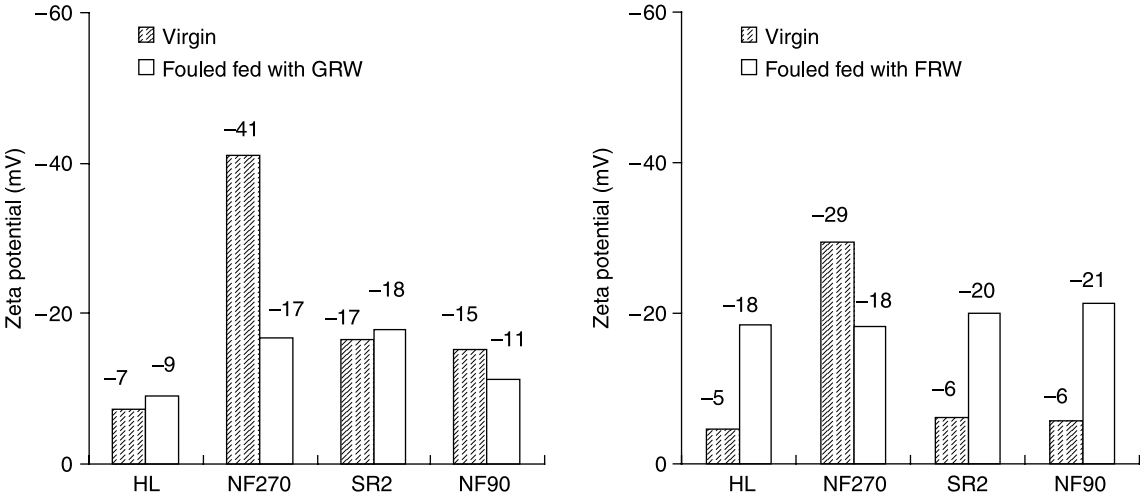

Figure 7 | Zeta potential of virgin and fouled membranes fed with GRW and FRW (data on left graph were determined using EKA, those on right graph were determined using SurPASS).

Table 3 | Thickness of the foulant layer and DOC loading

Parameter	NF90	HL	NF270	SR2
TFL with GRW (nm)	**2,762 ± 237** (2,319–3,531)	**1,820 ± 598** (634–3,155)	**3,562 ± 2,713** (527–9,087)	**3,845 ± 1,747** (1,612–6,755)
DOC loading (gC/m^2)	13	31	29	43
TFL with FRW (nm)	**1,858 ± 435** (1,128–2,919)	**2,302 ± 336** (1,560–3,106)	**2,992 ± 356** (2,351–3,844)	**3,062 ± 511** (2,180–4,115)
DOC loading (gC/m^2)	16	16	24	22

Notes: TFL, thickness of foulant layer; values in parentheses are the range. Both thickness and DOC loading were measured at the end of the experiment.

All fouled membranes, except NF90 and HL fed with GRW, possessed essentially identical zeta potentials (Figure 7). In addition to the similarity in contact angles noted above, the similar zeta potentials indicate that the foulant layer was similar regardless of water type and initial membrane characteristics.

The measured foulant layer thickness is reported in Table 3. The loose membranes (NF270 and SR2) showed thicker foulant layers compared to the tighter membranes (NF90 and HL). Tang *et al.* (2007) compared the foulant structure of three membranes at the same applied pressure. They found a thicker layer of humic acid for the more porous membrane, which was attributed to the higher initial flux for that membrane. In our study, different pressures were used to reach the same initial flux, indicating that parameters other than the initial flux seem to play a role in the thickness of the foulant layer. If the data for the HL membrane are not considered, there is a qualitative relationship between the thickness of the foulant layer and the DOC loading, especially for GRW. However, the

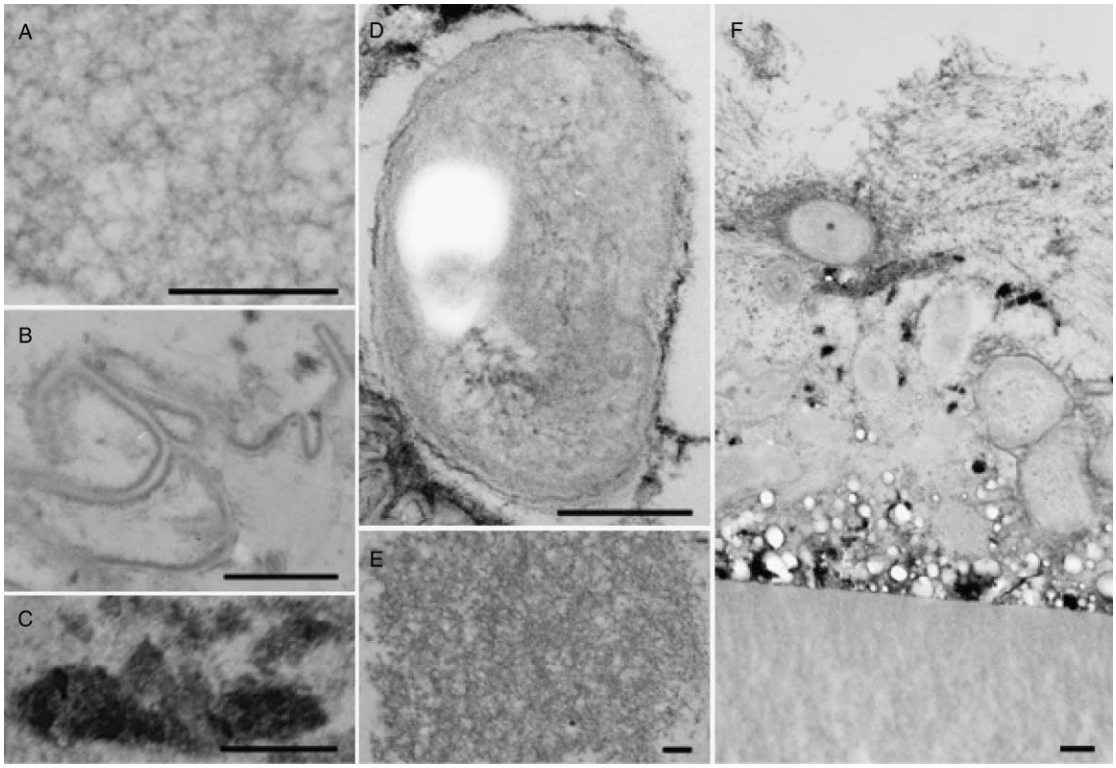

Figure 8 | Photographs of fibrils (A), cellular debris (B), inorganic foulants (C), bacterium (D), humics (E) and typical fouling layer on the active layer of all membranes (scale bar 200 nm).

generally large variability of the results precludes more quantitative interpretations. It is evident by comparing Table 3 with Figure 1 that a thicker fouling layer does not result in a greater flux decline. For example, in FRW, NF90 has the thinnest layer yet showed the greatest flux decline. SR2 had the thickest layer in both waters, yet showed the least flux decline.

Heterogeneity of the foulant layer

As noted previously, TEM alone and in combination with EDS were used to characterize the foulant layer. A systematic approach (Mavrocordatos *et al.* 2007; Leppard 2008) can provide structural information of the foulant materials based on shape, size and morphology, and also provide insight into their elemental composition. Figure 8F shows a TEM view of an ultrathin section of a fouled membrane, corresponding to a typical fouling layer found on the active layer of all membranes. The organic foulants identified are fibrils (Figure 8A) and probable humics (Figure 8E). Fibrils, which account for an important fraction of the NOM in natural fresh waters (up to 25%) (Wilkinson *et al.* 1997), are linear aggregates of biopolymers, usually rich in polysaccharides or polysaccharides plus proteins (Leppard 1997). Inorganic particles (Figure 8C), bacteria (Figure 8D) and cellular debris (Figure 8B) were

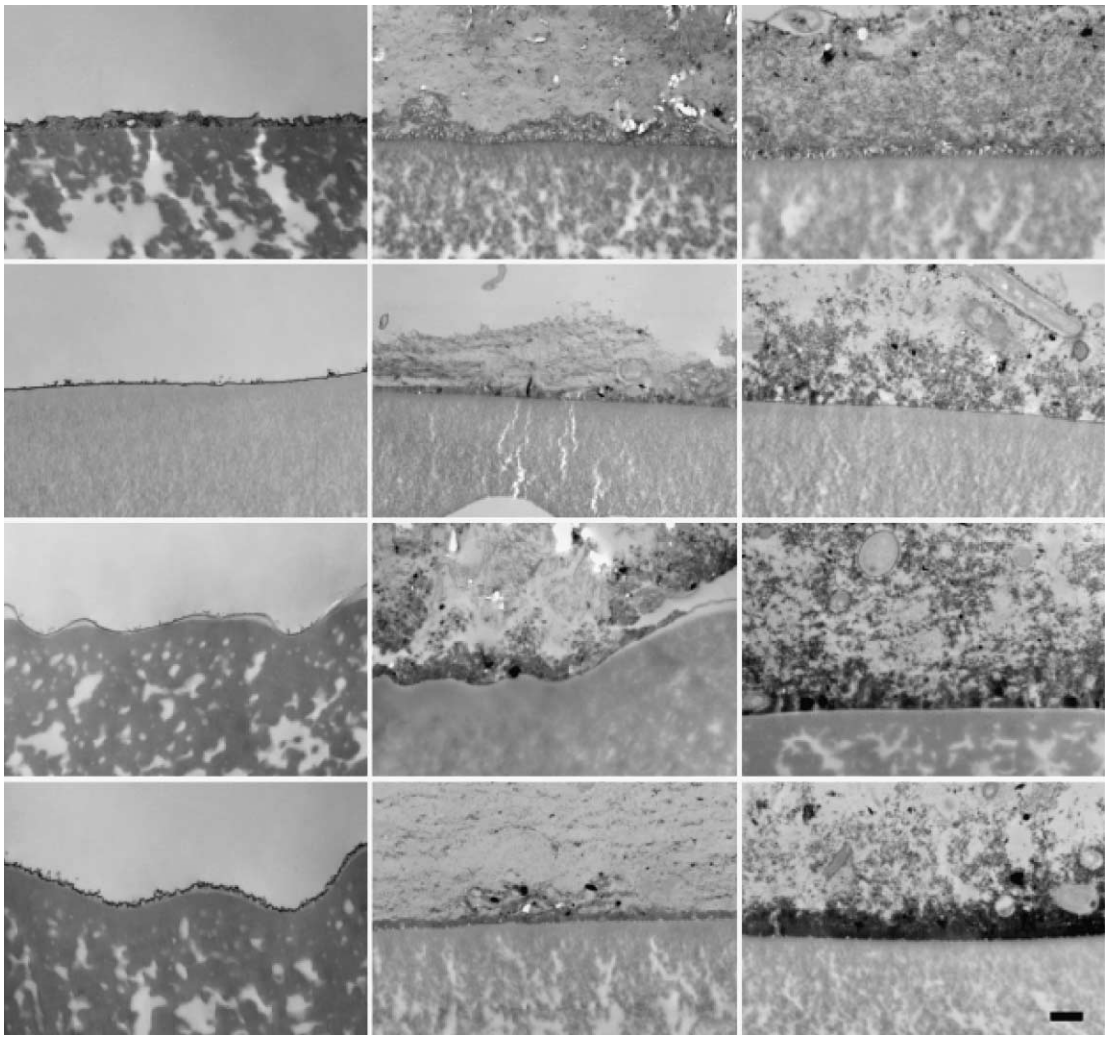

Figure 9 | TEM images (Magnification 10 K ×, scale bar 500 nm) of virgin membranes (first column), fouled membranes fed with GRW (second column) and fouled membranes fed with FRW (third column) (NF90, HL, NF270 and SR2 from top to bottom).

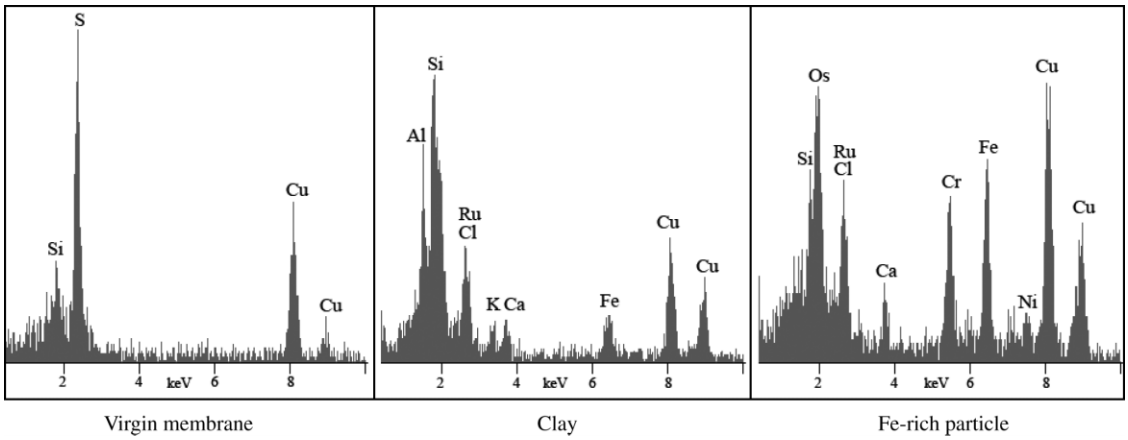

Figure 10 | EDS spectra of virgin NF90 membrane and particles located on the active layer after filtration of GRW (Y scale 200).

also identified according to standard images, using a guide to images provided by Leppard (1992). In contrast to AFM, which shows only a topographical image of the upper surface of a foulant layer, TEM offers the ability to distinguish between different nanoscale components comprising the foulant layer. An important overall message from Figure 8 is the great heterogeneity of the fouling layer.

TEM ultrastructural observations and STEM-EDS spectromicroscopy offer a unique benefit to distinguish between the different components comprising the foulant layer. Because of its nanoscale resolution (3 nm practical resolution for fouled membranes examined in epoxy-embedded ultrathin sections), TEM can reveal the extent and nature of association of the various aquatic classes of nanoscale particles that comprise the heterogeneous aggregated foulant in Figures 8 and 9. In fact, Buffle *et al.* (1998) have elucidated the generalized rules-of-the-game for understanding the interactions of the major types of aquatic nanoscale particles that result in mixed particle aggregates. Considering images such as that represented by Figure 8F, one finds that some of what appears to be humic substance fractal aggregates, as defined in terms of TEM images by Senesi (1999), can be a mixed aggregate in the foulant (containing also iron-rich nanoparticles, nanoscale mucilage fibrils and cell debris). Mixed nanoparticle aggregates can have unexpected properties and activities (Leppard 2008), thus confounding physico-chemical analyses of membrane–foulant interactions, which are based on the chemistry of a dominant foulant considered alone. This situation has important implications for the quantitative nanoscale modelling of the hydraulic impacts of fouling, for the selection or development of alternative membrane pretreatment or cleaning methods and for the selection or design of a membrane that would minimize fouling.

Figure 9 shows TEM images of the four virgin membranes and of each of them fouled with the two different waters. For the virgin membranes the figure shows the typical structure for a thin-film composite polyamide membrane: a dense polyamide active layer on top of a porous polysulfone support. Surprisingly the active layer thickness of the NF90 membrane (138 $\pm$ 33 nm) increased after experiments with GRW (280 $\pm$ 29 nm) and FRW (287 $\pm$ 57 nm). The active layer thickness of the other membranes remained the same after experiments using

Table 4 | Retention on day 3 of conductivity, silica and ions in the presence of fouling (GRW)

		Retention (%)								
Membrane	**Conductivity**	**SiO_2**	**K^+**	**Na^+**	**Ca^{2+}**	**Mg^{2+}**	**Mn^{2+}**	**Cl^-**	**NO_3^-**	**SO_4^{2-}**
NF90	94	73	100	58	86	82	100	66	42	91
HL	32	19	0	19	46	45	56	5	0	85
NF270	30	14	0	20	39	41	40	2	0	93
SR2	20	15	0	20	31	27	44	4	0	95

either water. It was found that the foulant materials were attached to the membrane surface and did not penetrate into the pores of the polysulfone support.

Further characterization of the inorganic foulants was investigated through EDS and by monitoring conductivity and ions in the feed and permeate samples. Figure 10 presents STEM-EDS spectra taken from a virgin NF90 membrane, and from two particles positioned on the active layer of that membrane, fed with GRW. These latter two spectra correspond to clay (Al, Si, K, Ca, Fe) and iron-rich particles. The spectra of the two particles also contain other elements such as Ca, Os, Cl and Cr. The detected Os is from the preparation method and Cl is (in part) a detectable component of the resin. Cr may have been leached from the filtration unit. In contrast, sulfur (S) is the main detectable element in the virgin membrane, while some of the Si might come from Formvar, which is used as a transparent film on top of the grid to provide support and improved stability for sections being analysed, which rest on the film during EDS analysis. The same inorganic deposits were observed on all membranes fed with both waters (data not shown), although the abundance of the elements differed from one membrane to another. These results help to illustrate the nanoscale heterogeneity of fouling.

Monitoring of conductivity in the feed and permeates throughout the fouling experiments confirmed that, with the exception of sulfate, the retention of inorganic constituents by the NF90 membrane was much greater than for the other membranes, as shown in Table 4 for GRW. For most constituents, the retention by the other three membranes was quite similar. Generally similar trends were seen for FRW (results not shown). The difference in removals by NF90 is due to its lower MWCO and tighter pore size, compared to the other membranes (Table 1). The retention of the inorganic constituents as illustrated by these data will also contribute to the heterogeneity of the fouling layer.

CONCLUSIONS

This study investigated the impact of water characteristics and membrane type on fouling of NF membranes by feeding two different surface waters to four different NF membranes. The major goal was to characterize the morphology and nanoscale ultrastructure of the fouled membranes and obtain information on the associated foulants, using a variety of techniques.

The major conclusions that can be drawn are:

1. On all four membranes a similar foulant layer 'took over' the properties of the virgin membranes. Thus the properties of initially quite different membranes tended to converge once they were fouled, which is of course their normal operating state in practice. Most of the fouled membranes had similar contact angles and zeta potentials, indicating that the major foulants were similar, despite the different initial membrane characteristics.
2. Similarly, the characteristics of the fouling layer were in general not greatly different for the two waters, despite major differences in the character of the organic matter and the concentrations of major inorganic ions in those waters. This conclusion and the one above have important implications for the use of nanofiltration in practice, including its application to remove trace contaminants such as pharmaceuticals and endocrine disrupting substances, where membrane surface properties may play an important role.
3. Transmission electron microscopy demonstrated that the fouling layer, although similar in bulk properties in all cases, was very heterogeneous. This has important implications for attempts to model quantitatively the impact of fouling on flux decline, for strategies to reduce fouling and for membrane cleaning approaches.
4. The nanoscale organic foulants identified using TEM were fibrils, linear aggregate of biopolymers usually rich in polysaccharide or polysaccharide plus protein and humics. Inorganic particles, such as clay and iron-rich particles, were also found. The major elements identified through EDS included Al, Ca, Fe, K and Si. Bacteria and cellular debris were also identified.
5. Virgin membrane properties other than pore size were not able to predict the rate or degree of fouling, thus confirming the complex nature of this phenomenon.

ACKNOWLEDGEMENTS

We sincerely thank Dow Filmtec for kindly providing NF90 and NF270 membranes and Koch Membrane

Systems for providing SR2 membranes. We would like to acknowledge Dr Yanxiao Yuan from Rensselaer Polytechnic Institute (Troy, NY, USA) and Dr Prajakta Kamerkar from Anton-Paar (Ashland, VA, USA) for performing zeta potential measurements. We also sincerely thank Dr G.A. Gagnon and Ms Heather Daurie of Dalhousie University for providing French River water, and Ms Dana Herriman of the NSERC Chair for assistance with manuscript preparation. Funding for this project was provided by the Natural Sciences and Engineering Research Council of Canada (NSERC) in the form of an Industrial Research Chair (IRC) program and the Canadian Water Network (CWN). The current Chair partners can be found at http://www.civil.uwaterloo.ca/watertreatment.

REFERENCES

Allgeier, S. C. & Summers, R. S. 1995 Evaluating NF for DBP control with RBSMT. *J. AWWA* **87**(3), 87–99.

Amy, G. & Cho, J. 1999 Interactions between natural organic matter (NOM) and membranes: rejection and fouling. *Water Sci. Technol.* **40**(9), 131–139.

Buffle, J., Wilkinson, K. J., Stoll, S., Filella, M. & Zhang, J. 1998 A generalized description of aquatic colloidal interactions: the three-colloidal component approach. *Environ. Sci. Technol.* **32**, 2887–2899.

Chandler, J. A. 1977 *X-ray Microanalysis in the Electron Microscope*. North-Holland Publ. Co., Amsterdam, The Netherlands.

Cho, J., Amy, G. & Pellegrino, J. 2000 Membrane filtration of natural organic matter: comparison of flux decline, NOM rejection, and foulants during filtration with three UF membranes. *Desalination* **127**(3), 283–298.

Haberkamp, J. 2008 *Organisches Membranfouling bei der Ultrafiltration kommunaler Kläranlagenabläufe-Ursachen, Mechanismen und Maßnahmen zur Verringerung (Organic Membrane Fouling during Ultrafiltration of Treated Wastewater Effluents, Mechanisms and Measures for Fouling Reduction)*. PhD Dissertation, Technical University of Berlin, Berlin, Germany, http://opus.kobv.de/tuberlin/volltexte/2009/2107/pdf/haberkamp_jens.pdf

Haberkamp, J., Ruhl, A. S., Ernst, M. & Jekel, M. 2007 Impact of coagulation and adsorption on DOC fractions of secondary effluent and resulting fouling behaviour in ultrafiltration. *Water Res.* **41**, 3794–3802.

Hallé, C., Huck, P. M., Peldszus, S., Haberkamp, J. & Jekel, M. 2009 Assessing the performance of biological filtration as pretreatment to low pressure membranes for drinking water. *Environ. Sci. Technol.* **43**(10), 3878–3884.

Her, N., Amy, G., Plottu-Pecheux, A. & Yoon, Y. 2007 Identification of nanofiltration membrane foulants. *Water Res.* **41**, 3936–3947.

Hobbs, C., Hong, S. & Taylor, J. 2006 Effect of surface roughness on fouling of RO and NF membranes during filtration of a high organic surficial groundwater. *J. Water Supply Res. Technol.–AQUA* **55**(7–8), 559–570.

Hong, S. & Elimelech, M. 1997 Chemical and physical aspects of natural organic matter (NOM) fouling of nanofiltration membranes. *J. Membr. Sci.* **132**, 159–181.

Huang, H., Lee, N.-H., Young, T., Amy, G., Lozier, J. C. & Jacangelo, J. G. 2007 Natural organic matter fouling of low-pressure, hollow-fiber membranes: effects of NOM source and hydrodynamic conditions. *Water Res.* **41**(17), 3823–3832.

Jackson, T. A. & Leppard, G. G. 2002 Energy dispersive X-ray microanalysis and its applications in biogeochemical research. In: Violante, A., Huang, P. M., Bollag, J.-M. & Gianfreda, L. (eds) *Soil Mineral-Organic Matter-Microorganism Interactions and Ecosystem Health*. Elsevier, Amsterdam, The Netherlands, pp. 219–260.

Košutić, K., Dolar, D. & Kunst, B. 2006 On experimental parameters characterizing the reverse osmosis and nanofiltration membranes' active layer. *J. Membr. Sci.* **282**(1–2), 109–114.

Lankes, U., Müller, M. B., Weber, M. & Frimmel, F. H. 2009 Reconsidering the quantitative analysis of organic carbon concentrations in size exclusion chromatography. *Water Res.* **43**(4), 915–924.

Lee, S. & Elimelech, M. 2006 Relating organic fouling of reverse osmosis membranes to intermolecular adhesion forces. *Environ. Sci. Technol.* **40**, 980–987.

Leppard, G. G. 1992 Evaluation of electron microscope techniques for the description of aquatic colloids. In: Buffle, J. & van Leeuwen, H. P. (eds) *Environmental Particles*, (Vol. 1). Lewis Publisher, Chelsea, MI, USA, pp. 231–289.

Leppard, G. G. 1997 Colloidal organic fibrils of acid polysaccharides in surface waters: electron-optical characteristics, activities and chemical estimates of abundance. *Colloids Surf. A* **120**, 1–15.

Leppard, G. G. 2008 Nanoparticles in the environment as revealed by transmission electron microscopy: detection, characterisation and activities. *Curr. Nanosci.* **4**, 278–301.

Leppard, G. G., Droppo, I. G., West, M. M. & Liss, S. N. 2003 Compartmentalization of metals within the diverse colloidal matrices comprising activated sludge microbial flocs. *J. Environ. Qual.* **32**, 2100–2108.

Li, Q., Xub, Z. & Pinnau, I. 2007 Fouling of reverse osmosis membranes by biopolymers in wastewater secondary effluent: role of membrane surface properties and initial permeate flux. *J. Membr. Sci.* **290**, 173–181.

Liao, B. Q., Bagley, D. M., Kraemer, H. E., Leppard, G. G. & Liss, S. N. 2004 A review of biofouling and its control in membrane separation bioreactors. *Water Environ. Res.* **76**, 425–436.

Liss, S. N., Droppo, I. G., Flannigan, D. T. & Leppard, G. G. 1996 Floc architecture in wastewater and natural riverine systems. *Environ. Sci. Technol.* **30**, 680–686.

Mackey, E. D. 1999 *Fouling of Ultrafiltration and Nanofiltration Membranes by Dissolved Organic Matter*. Dissertation, Rice University, Environmental Science and Engineering, Houston.

Makdissy, G., McPhail, B. & Peldszus, S. 2009 Removal of selected EDCs and pharmaceuticals and PCPs from surface waters by nanofiltration (in preparation).

Mavrocordatos, D., Perret, D. & Leppard, G. G. 2007 Strategies and advances in the characterisation of environmental colloids by electron microscopy. In: Wilkinson, K. J. & Lead, J. R. (eds) *Environmental Colloids and Particles: Behaviour, Separation and Characterisation*. John Wiley & Sons, Chichester, UK, pp. 345–404.

Nghiem, L. D. & Hawkes, S. 2007 Effects of membrane fouling on the nanofiltration of pharmaceutically active compounds (PhACs): mechanisms and role of membrane pore size. *Sep. Purif. Technol.* **57**, 182–190.

Nghiem, L. D., Schäfer, A. I. & Elimelech, M. 2004 Removal of natural hormones by nanofiltration membranes: measurement, modeling and mechanisms. *Environ. Sci. Technol.* **38**(6), 1888–1896.

Roudman, A. R. & DiGiano, F. A. 2000 Surface energy of experimental and commercial nanofiltration membranes: effects of wetting and natural organic matter fouling. *J. Membr. Sci.* **175**(1), 61–73.

Senesi, N. 1999 Aggregation patterns and macromolecular morphology of humic substances: a fractal approach. *Soil Sci.* **164**, 841–856.

Tang, C. Y., Kwon, Y.-N. & Leckie, J. O. 2007 Fouling of reverse osmosis and nanofiltration membranes by humic acid–effects of solution composition and hydrodynamic conditions. *J. Membr. Sci.* **290**, 86–94.

Teixeira, M. R. & Rosa, M. J. 2006 The impact of the water background inorganic matrix on the natural organic matter removal by nanofiltration. *J. Membr. Sci.* **279**(1–2), 513–520.

Tran, T., Bolto, B., Gray, S., Hoang, M. & Ostarcevic, E. 2007 An autopsy study of a fouled reverse osmosis membrane element used in a brackish water treatment plant. *Water Res.* **41**(17), 3915–3923.

Van der Bruggen, B. & Vandecasteele, C. 2001 Flux decline during nanofiltration of organic components in aqueous solution. *Environ. Sci. Technol.* **35**(17), 3535–3540.

Wilkinson, K. J., Joz-Roland, A. & Buffle, J. 1997 Different roles of pedogenic fulvic acids and aquagenic biopolymers on colloid aggregation and stability in freshwaters. *Limnol. Oceanogr.* **42**, 1714–1724.

Xu, P., Drewes, J. E. & Kim, T. U. 2006 Effect of membrane fouling on transport of organic contaminants in NF/RO membrane applications. *J. Membr. Sci.* **279**, 165–175.

Yamamura, H., Chae, S., Kimura, K. & Watanabe, Y. 2007 Transition in fouling mechanism in microfiltration of a surface water. *Water Res.* **41**(17), 3812–3822.

Ye, Y., Le Clech, E., Chen, V., Fane, A. G. & Jefferson, B. 2005 Fouling mechanisms of alginate solutions as model extracellular polymeric substances. *Desalination* **175**, 7–20.

Yuan, W. & Zydney, A. L. 2000 Humic acid fouling during ultrafiltration. *Environ. Sci. Technol.* **34**(23), 5043–5050.

First received 19 June 2009; accepted in revised form 18 December 2009